Environmental Science Nano

PAPER

View Article Online
View Journal | View Issue

Cite this: *Environ. Sci.: Nano*, 2015, 2, 68

Accumulation, speciation and uptake pathway of ZnO nanoparticles in maize†

Jitao Lv,[a] Shuzhen Zhang,*[a] Lei Luo,[a] Jing Zhang,[b] Ke Yang[c] and Peter Christie[d]

Received 9th April 2014,
Accepted 15th September 2014

DOI: 10.1039/c4en00064a

rsc.li/es-nano

Engineered nanomaterials such as ZnO nanoparticles (NPs) will inevitably enter the environment because of the large quantities produced and their widespread application. Plants comprise a fundamental living component of terrestrial ecosystems; thus, understanding the interaction between ENMs and plants is important. In the present study we conducted an integrated study by employing a combination of microscopic and spectroscopic techniques to comparatively investigate the uptake of ZnO NPs and Zn^{2+} ions by maize in order to further elucidate plant uptake pathways of ZnO NPs. The results demonstrate that the majority of Zn taken up was derived from Zn^{2+} released from ZnO NPs, and Zn accumulated in the form of Zn phosphate. ZnO NPs were observed mainly in the epidermis, a small fraction of ZnO NPs were present in the cortex and root tip cells, and some further entered the vascular system through the sites of the primary root–lateral root junction. However, no ZnO nanoparticle was observed to translocate to shoots, possibly due to the dissolution and transformation of ZnO NPs inside the plants.

Nano impact

ZnO nanoparticles (NPs), one of the most common engineered nanomaterials, have been used widely in many fields. Thus, the potential of their release into the environment and the subsequent impacts on the environment and human health have raised much concern. Plants provide a potential pathway for the transport of ZnO NPs in the environment and serve as an important route for their bioaccumulation in the human food chain. In the present study, a combination of microscopic and spectroscopic characterization techniques was used to investigate the uptake pathway, accumulation speciation, and cellular localization of ZnO NPs in maize. The results demonstrate that the majority of Zn taken up was derived from Zn^{2+} released from ZnO NPs and Zn accumulated in the form of Zn phosphate. ZnO NPs were observed mainly in the epidermis, a small fraction of ZnO NPs further entered the vascular system through the sites of the primary root–lateral root junction.

1. Introduction

The past decade has witnessed an exponential growth in nanotechnology with the manufacture of different types of engineered nanomaterials (ENMs) on the large scale for both industrial and household purposes. The potential for their release into the environment and the subsequent impacts on the environment and human health have raised considerable concern.[1–3]

Plants comprise a fundamental living component of terrestrial ecosystems. Moreover, plant uptake, translocation and accumulation of ENMs may pose a threat to the safety of the human food chain.[4–6] However, plant uptake of ENMs is a very recent field of study and contradictory results have been reported, with some studies reporting plant accumulation of ENMs[7,8] and others showing no uptake.[9–13] Therefore, an attempt must be made to elucidate the pathways and mechanisms of NP uptake by plants to explain the contradictory observations regarding plant uptake. One of the most important distinguishing features of plant cells is that they are enclosed by rigid cell walls composed of cellulose, hemicelluloses and pectin with pores whose diameter is typically in the range of 3–8 nm,[14] and these allow only small molecules to pass through. Navarro *et al.* therefore hypothesized that only nanoparticles with a size smaller than the pores of cell walls can pass through and reach the plasma membrane.[4] However, many studies have shown that not only small NPs[12,15–17] such as TiO_2, C_{70}, $C_{60}(OH)_{20}$ and Au with diameters of <5 nm, but also larger NPs were taken up by

[a] *State Key Laboratory of Environmental Chemistry and Ecotoxicology, Research Center for Eco-Environmental Sciences, Chinese Academy of Sciences, Beijing 100085, China. E-mail: szzhang@rcees.ac.cn; Fax: +86 10 62923563; Tel: +86 10 62849683*
[b] *State Key Laboratory of Synchrotron Radiation, Institute of High Energy Physics, Chinese Academy of Sciences, Beijing 100039, China*
[c] *Shanghai Institute of Applied Physics, Chinese Academy of Sciences, Shanghai, 201800, China*
[d] *Agri-Environment Branch, Agri-Food and Biosciences Institute, Newforge Lane, Belfast BT9 5PX, UK*

† Electronic supplementary information (ESI) available. See DOI: 10.1039/c4en00064a

plant roots or even transported into the aerial parts of plants.[18–20] It is still unclear through which route the NPs pass through the cell walls and are internalized by plant cells to undergo vascular transport in plants, or how these particles pass through the Casparian strip, a belt of specialized cell wall material that generates an extracellular diffusion barrier around the vascular cylinder.[21] It is necessary to address these important issues to elucidate the pathways and mechanisms of plant uptake and translocation of NPs, which are still far from clear.[22]

ZnO NPs are amongst the most common engineered nanomaterials. They are used widely in many applications and consequently can be released into the environment.[23] Research by Gottschalk *et al.* has indicated that the environmental concentrations of ZnO NPs are second only to those of TiO_2.[24] This raises the urgent need to understand the behaviors and effects of ZnO NPs in the environment. Disposal of municipal solid wastes may provide an important pathway for plant exposure to ZnO NPs due to the increasing commercialization of ENMs. Lin *et al.* have studied the phytoaccumulation and phytotoxicity of ZnO nanoparticles at a concentration of 1000 mg L^{-1} and observed the distribution of ZnO NPs in wheat roots by transmission electron microscopy (TEM),[25] whereas Lopez-Moreno *et al.* reported that there were no ZnO NPs found in soybean (*Glycine max*) roots by synchrotron X-ray absorption spectroscopy (XAS), even at a high concentration of ZnO NPs (4000 mg L^{-1}).[26] Similarly, Hernandez-Viezcas *et al.* demonstrated that ZnO NPs were not present in mesquite tissues, and Zn was found in a form resembling $Zn(NO_3)_2$.[13] Recently, Hernandez-Viezcas *et al.* studied the location and speciation of ZnO and CeO_2 nanoparticles taken up by soybean (*Glycine max*) using micro-X-ray fluorescence analysis (μ-XRF) and micro-X-ray absorption near-edge spectroscopy (μ-XANES), and their results showed that Zn accumulated in a form resembling Zn citrate in soybean under treatment with ZnO NPs.[28] However, Zhao *et al.*, by using a confocal microscope, studied the uptake of FITC-stained ZnO NPs by corn plants growing in a sandy loam soil, and they observed that ZnO NP aggregates penetrated the root epidermis and cortex through the apoplastic pathway. The presence of ZnO NP aggregates in xylem vessels suggested that the aggregates passed the endodermis through the symplastic pathway.[27] However, more information is necessary to validate such conclusions, considering the limitations of confocal microscopy. Moreover, although the uptake of ZnO NPs was involved in these studies, there are still some questions that need to be further investigated. For example, whether Zn accumulated in plants was from the uptake of ZnO NPs or Zn^{2+} ions was still unclear since these studies lacked Zn^{2+} treatment as comparison. If the uptake of ZnO NPs by plants exists, it is necessary to elucidate the route through which they enter plants and in what form they accumulate in plants. Therefore, a combination of microscopic and spectroscopic characterization techniques comprising synchrotron-based XAS and μ-XRF analyses, optical fluorescence microscopic tracking of labeled ZnO NPs and transmission electron microscopy (TEM) imaging was employed to investigate the uptake pathway, accumulation, speciation, and cellular localization of ZnO NPs in maize. The role of the dissolution of ZnO NPs in their uptake by maize was also investigated in detail.

2. Materials and methods

2.1 Preparation of exposure suspension

ZnO NPs were purchased from Na Chen Scientific & Technical Co., Beijing, China. The size distribution, crystal structure, surface charge, specific surface area and aggregation state of ZnO NPs were measured, and the detailed methods are provided in the ESI.† Suspensions of ZnO NPs were prepared at 0, 2, 5, 10, 15, 20, 40, 60, 80 and 100 mg L^{-1} (particle concentration) in 1% modified Hoagland solution, stirred for 30 min, sonicated for 30 min, and then continuously stirred for 30 min to avoid sedimentation. $ZnSO_4$ at various concentrations (Zn concentrations of 1, 1.5, 3, 6, 8, 10, 15, 20, 25, 30, 40, 50, 64 and 80 mg L^{-1}) dissolved in 1% modified Hoagland solution was prepared for plant exposure to Zn^{2+} in solution. The pH of each suspension was adjusted to 6.8 ± 0.2 before plant exposure. 10 mL of each ZnO NP suspension at various concentrations was shaken at 100 rpm for 24 h at room temperature, aiming to dissolve ZnO NPs. Then the dissolved Zn^{2+} and ZnO NPs were separated by centrifugation at 20 000*g* for 40 min followed by filtration through 0.025 μm microporous membranes (Millipore). The filtrates were acidified with 100 μL of HNO_3 (pure) and quantified by ICP-OES (Optima 2000DV, Perkin Elmer). High quantitative recovery of Zn^{2+} (96–100%) was obtained by examining a series of solutions with different soluble Zn^{2+} concentrations using the above procedure, indicative of negligible retention of Zn^{2+} by the membrane. Therefore, the Zn present in filtrates was considered as dissolved Zn released from ZnO NPs.

2.2 Hydroponic cultivation and exposure experiments

Maize (*Zea mays* L. cv. Zhengdan 958) was used as the test species. Seeds were purchased from the Chinese Academy of Agricultural Sciences, Beijing, China. Hydroponics was used for plant cultivation and exposure. The seedlings were grown in 50% Hoagland nutrient solution for 7 days with 16 h of simulated sunshine per day provided by supplementary illumination (light intensity of 250 μmol m^{-2} s^{-1}) at a temperature of 25–30 °C, and a night (8 h) temperature of 15–20 °C before the exposure study (details provided in the ESI†). After 7 days of hydroponic cultivation, maize seedlings were exposed to the ZnO NP suspensions or Zn^{2+} solutions described above. The exposure suspensions or solutions were renewed daily and the exposure lasted for 7 days. After plant exposure, the suspension pH showed only a slight change (ranging from 6.6 to 7.2) and no subsequent pH adjustments were then performed. The filtrates (soluble Zn^{2+}) of ZnO suspensions after plant exposure were separated, and the Zn^{2+} concentrations were measured by the same method as described above. Plant tissue samples were lyophilized, and

then 0.1000 g samples were digested using HNO_3 and $HClO_4$ (4 : 1) following the method of Yu *et al.*[29] Zn concentrations were then quantified by ICP-OES. A tea standard reference material, GBW 10016, obtained from the Center of National Standard Reference Material of China, was analyzed and good agreement was achieved between the data obtained from the present study and the certified values, with recoveries between 93% and 105%.

2.3 Sample preparation for microscopy and μ-XRF analysis

Fresh seedlings grown in 100 mg of ZnO NPs per liter of solution ZnO NPs or 30 mg of Zn^{2+} per liter of solution for 7 days were washed with deionized water three times and divided into roots, stems and leaves. Samples were then preserved in liquid nitrogen for at least 1 h. Sections (40 μm thick) of samples were cut with a Leica CM1850 cryostat at −20 °C using deionized water as the embedding medium to minimize possible effects of the embedding medium on Zn speciation. To maintain the plant tissues intact and suitable for μ-XRF analysis, the method developed by Lombi *et al.* was used.[30] Simply, a piece of Kapton tape (3M, USA) was pressed on the top of the sample, with the blade of the microtome cutting underneath. In this way, 40 μm thick sections were obtained directly on Kapton tape, and then a piece of Kapton tape was overcast on the other side of the section as soon as possible. Sections were placed in the cryostat until dry and those in good condition were selected for μ-XRF mapping. For optical fluorescence microscopic observation, 20 μm tissue sections of seedlings exposed to a 100 mg L^{-1} ARS-ZnO NP suspension, 10 mM ARS and deionized water were prepared by the same method as the above except using optimum cutting temperature compound (Tissue-Tek® O.C.T. Compound, Sakura Finetek, Torrance, CA) as the embedding medium instead of deionized water.

2.4 Synchrotron X-ray absorption spectrum and μ-XRF microprobe analysis

For XAS analysis, fresh maize seedlings were first preserved in liquid nitrogen and then lyophilized at −40 °C for 48 h. 0.0300 g samples of lyophilized powder of roots or shoots of maize seedlings exposed to 100 mg L^{-1} ZnO NPs or 30 mg L^{-1} Zn^{2+} were pressed into pellets. The pellets were pasted on Kapton tape (3M, USA) and then subjected to XAS analysis. Zinc K-edge X-ray absorption spectra were collected at room temperature at the 1W1B beamline of the Beijing Synchrotron Radiation Facility (Beijing, China). The energy of the Zn K-absorption edge (9659 eV) was calibrated with Zn foil, and an energy range of −200 to 800 eV from the K-edge of Zn was used to acquire the spectra. ZnO NPs, Zn phosphate (hopeite), Zn phytate, Zn-sorbed hydroxyapatite to represent amorphous Zn phosphate (Zn_{ads}-Phos),[31] ZnS, Zn citrate, Zn malate and $ZnSO_4$ aqueous solution were used as reference compounds. Data for the samples and liquid reference compounds were collected in fluorescence mode under ambient conditions, and those for the solid reference compounds were collected in transmission mode. Two to three scans were performed on average to achieve an adequate signal/noise ratio. Standard XAFS data reduction procedures were undertaken using the program package IFEFFIT,[32] and WinXAS version 3.1 (ref. 33) was used for EXAFS fitting. XANES data (average of two or three scans) of the samples were analyzed by linear combination fitting (LCF) using Athena software.[34] More detailed information about data analysis is provided in the ESI.†

Synchrotron μ-XRF microprobe maps of 40 μm cross and longitudinal sections prepared as described above were obtained at room temperature at the beamline 15U at the Shanghai Synchrotron Radiation Facility (SSRF). Incident X-rays of 10.02 keV were used to excite elements in the prepared samples. The electron energy in the storage ring was 3.5 GeV with a current ranging from 120 mA to 210 mA. The microfocused beam of about 10 μm was provided by a K-B lens with the sample at 45° to the incident X-ray beam. The fluorescence yield was detected using a 7-element Si (Li) solid-state detector (E2V Scientific Instruments Ltd.) positioned at 90° to the beamline. The dwell time per point was 1 s and the step size was set to 15 μm to 25 μm depending on the size of the area mapped. The fluorescence intensities of Zn, K, Ca, Fe, Mn, Cu and Compton scattering were recorded simultaneously. The fluorescence intensity was normalized by I_0 and dwell time to correct for the effect of synchrotron radiation beam flux variation on the signal intensity. More detailed information about data analysis is provided in the ESI.†

2.5 Fluorescence tracking and TEM analysis

ZnO NPs (10 mM) stored in citrate buffer (100 mM, pH 6.5) were mixed with Alizarin red S (50 mM) and shaken at 100 rpm for 24 h at room temperature, and then the samples were centrifuged at 20 000*g* for 1 h. The supernatants were discarded and the residues were washed with deionized water until the supernatants were almost colorless. The residues were retained, lyophilized and ground, and purple powders of alizarin red S-labeled ZnO NPs (ARS-ZnO NPs) were finally obtained. Maize seedlings were exposed to a suspension of 100 mg L^{-1} ARS-ZnO NPs and a solution of 10 mM ARS. Fluorescence microscopic images of the different sections of plant tissues were observed using an inverted phase-contrast fluorescence microscope (Zeiss Axiovert 200, Germany).

To image the cellular localization of ZnO NPs in root cells, tissue sections of maize exposed to solutions with and without ZnO NPs were prepared by fixation, gradual dehydration, embedment, polymerization, and ultrathin sectioning (70 nm) and were stained and examined by TEM (JEOL JEM 1010, Tokyo, Japan). Method details are provided in the ESI.†

3. Results

3.1 ZnO nanoparticle characterization

The purity of ZnO NPs (no surface coating) used in this study was 99.9% with a surface area of 29 ± 1 m^2 g^{-1}. XRD patterns

revealed that the crystalline phase of the ZnO nanoparticles was consistent with that of zincite. TEM micrographs indicated that the primary ZnO NPs were nearly spherical with diameters of 30 ± 5 nm, obtained by measuring over 200 single particles. The isoelectric point (IEP) of ZnO NPs is 9.1 ± 0.2, indicative of positive surface charges at neutral pH. Dynamic light scattering analysis indicated that ZnO NPs tended to aggregate and exhibited a mean hydrodynamic diameter of around 450 nm with a wide range (Fig. S1 in the ESI†).

3.2 Accumulation of Zn in maize under exposure to ZnO NPs

Dissolution of ZnO NPs at various concentrations over 24 h with and without plant exposure was measured first. As shown in Fig. 1A, the concentrations of dissolved Zn^{2+} increased with increasing particle density of ZnO NPs in the hydroponic medium in both cases, but much higher Zn^{2+} concentrations were detected in the presence of plants, especially at high particle densities (Fig. S2†). Then comparative plant accumulation experiments were conducted by parallel exposure of maize to ZnO NPs and Zn^{2+}. After 7 days of exposure, the concentrations of Zn in roots and shoots increased quickly with increasing concentrations of Zn^{2+} or ZnO NPs below 5 mg L^{-1} (dissolved Zn), followed by an apparent steady state in shoots and a slow increase in roots (Fig. 1B). It is interesting to note that shoot Zn concentrations under exposure to ZnO NPs and Zn^{2+} overlapped each other when the dissolved Zn^{2+} concentrations calculated based on the dissolution ratios of ZnO NPs at different particle densities were considered. Root Zn concentrations under the two treatments were also similar to each other, but differences were present in the treatments with ZnO NPs at high particle densities.

3.3 Speciation of Zn in maize under exposure to ZnO NPs

XAS analysis was conducted to elucidate Zn speciation in roots and shoots of maize seedlings exposed to 30 mg L^{-1} (Zn concentration) $ZnSO_4$ and 100 mg L^{-1} ZnO NPs (dissolved Zn 31.4 ± 1.7 mg L^{-1}). Zn K-edge XANES and EXAFS spectra of the reference compounds and the plant samples are shown in Fig. 2. LCF was performed on the XANES spectra of the samples (Fig. 2D) using the spectra of Zn phosphate species including Zn hopeite and Zn_{ads}-Phos, considering their similarity to the main features of the XAS spectra of the plant samples. Phytate Zn was not included because it shares XAS spectra identical to those of hopeite (Fig. 2A, B, C).[35] Standard spectra of other compounds among the reference chemicals were then added in the fitting. However, only the addition of the spectra of ZnO significantly improved the quality of fit (the normalized sum of square values decreased by at least 10%). The LCF results (Table S1†) showed a high proportion (76–95%) of zinc phosphate complexes (in both inorganic and organic forms) present in the plant samples, with zinc phosphate (hopeite or Zn phytate) as the major species in shoots (70–83%) and Zn_{ads}-Phos in roots (69–76%). The percentage of ZnO(H) in roots (24%) treated with ZnO NPs was over four times more than that in the other plant samples (Table S1†).

3.4 Distribution of Zn in maize under exposure to ZnO NPs

Synchrotron μ-XRF microprobe mapping, which enables direct *in situ* quantitative visualization of the elemental distribution in plant tissues, was employed to observe the spatial distribution of Zn in maize. Fig. 3 shows the distribution of Zn in root, stem, and leaf cross sections (optical photographs are provided in Fig. S3†) of maize exposed to 30 mg L^{-1} $ZnSO_4$ or 100 mg L^{-1} ZnO NPs (dissolved Zn 31.4 ± 1.7 mg L^{-1}). The μ-XRF maps displayed distinct similarities in both distribution and content of Zn in the leaves and stems under the two treatments (comparison between Fig. 3A and D, and between 3B and E). However, more hot points (representing Zn accumulation) in the root cortex were found for the treatment with ZnO NPs than that with Zn^{2+} (Fig. 3C and F).

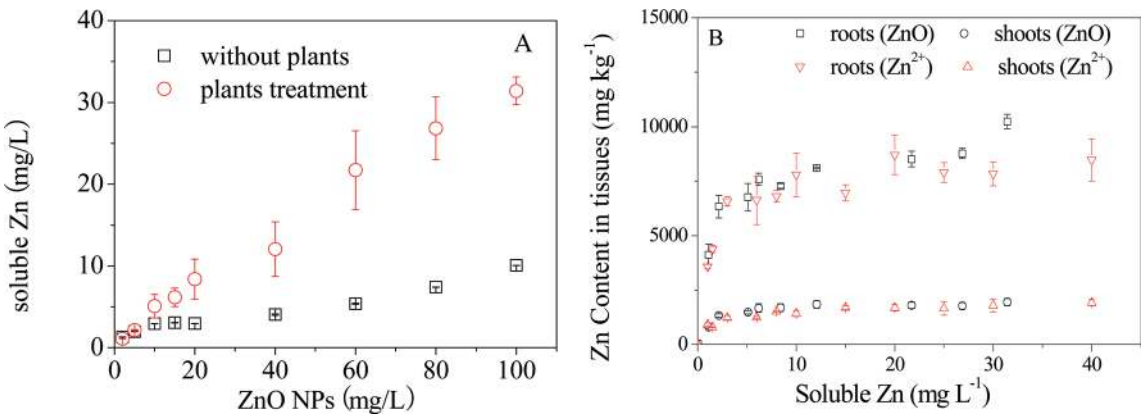

Fig. 1 Comparative dissolution of ZnO NPs with and without plants over 24 h (A); Zn accumulation in shoots and roots of maize exposed to Zn^{2+} and ZnO NPs for 7 days (B); soluble Zn in (B) represents the dissolved concentrations of Zn^{2+} released from ZnO NPs.

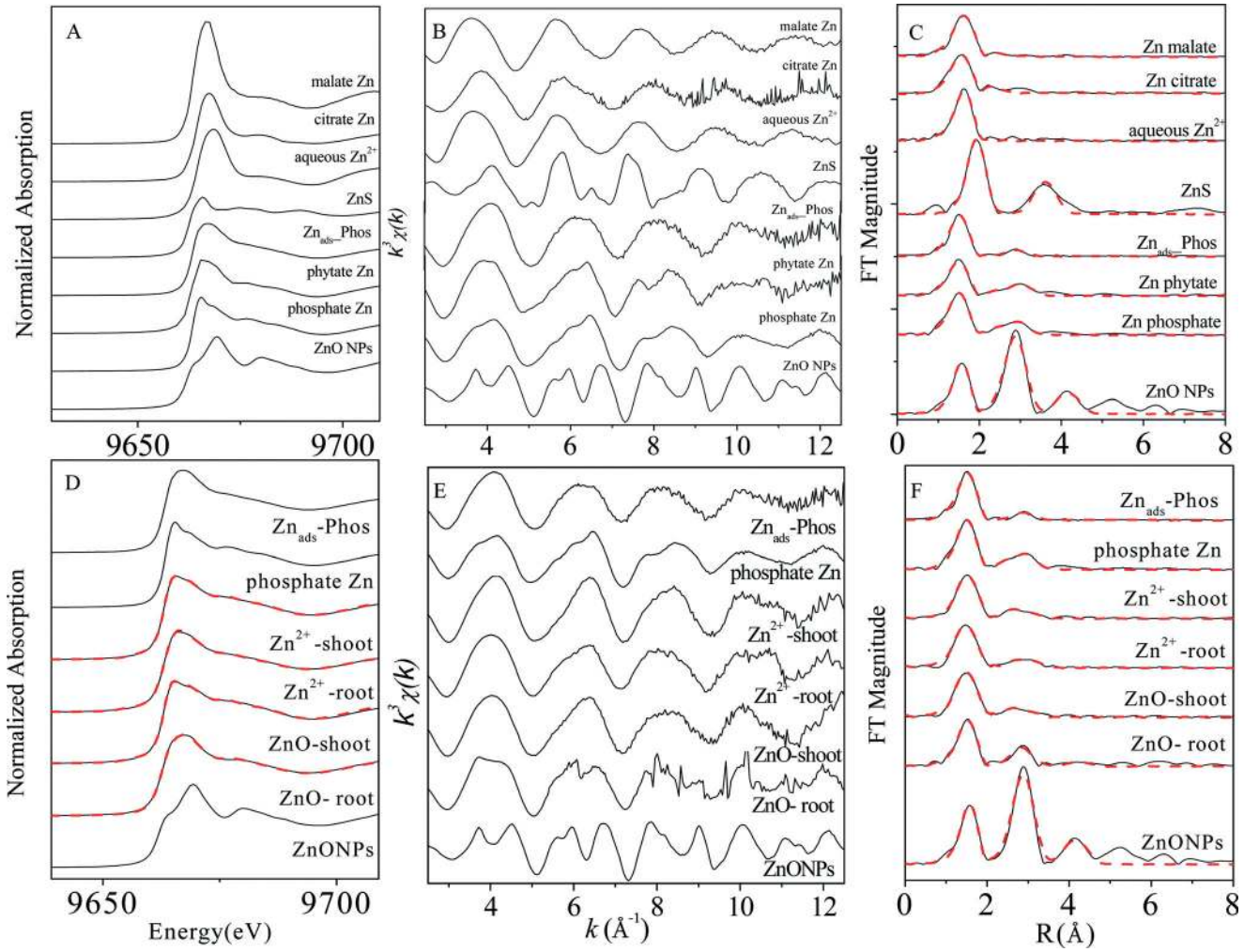

Fig. 2 Normalized Zn K-edge XANES spectra (A), k^3-weighted EXAFS data (B) and corresponding radial distribution functions (RDF) obtained by Fourier transformation of the EXAFS spectra (C) of the model compounds; normalized Zn K-edge XANES spectra (D), k^3-weighted EXAFS data (E) and corresponding radial distribution functions (RDF) obtained by Fourier transformation of the EXAFS spectra (F) of plant samples. Solid lines represent experimental data, dashed lines represent fitted data.

3.5 Localization of nanoparticles in maize

Fluorescence labeling and TEM imaging were used to investigate the localization of nanoparticles in maize. Alizarin red S (ARS) has been used as a fluorescent marker for many metal oxide NPs,[35] and ARS-labeled TiO_2 NPs have been further successfully used to track the translocation of TiO_2 NPs in both cancer cells and plants.[15,36] Therefore, ARS-labeled ZnO NPs (ARS-ZnO NPs) were prepared to track the distribution of ZnO NPs inside maize. These ARS-ZnO NP aggregates appeared purple when observed by the naked eye and emitted bright orange fluorescence using a violet filter (excitation wavelength 395–415 nm), while ARS alone that accumulated in the roots displayed a purple color (Fig. S4†). As shown in Fig. 4, the blue color represented the background autofluorescence of plant tissues, while ARS-ZnO NPs and their aggregates appeared as light orange dots (indicated by arrows). Numerous light orange particles adhered to the root surface of maize after exposure to ARS-ZnO NPs (Fig. 4A), indicating a strong affinity of ARS-ZnO NPs for the root surface. In order to track the translocation of ARS-ZnO NPs inside maize, both 20 μm cross and longitudinal sections of roots were imaged. Orange dots of different sizes were observed inside the epidermis and cortex but none was observed in the root vascular systems (Fig. 4B and C). However, a much higher intensity of orange color appeared at the primary root–lateral root junction than in other regions (Fig. 4D–I). Furthermore, none was observed in the shoots (Fig. S4†).

Fig. 5 gives the TEM images of root sections in different zones after maize was exposed to 100 mg L^{-1} ZnO NPs. Integrated cellular structures with no obvious dense dots were observed in the roots without exposure to ZnO NPs (Fig. 5A). However, copious dense dots were observed in the intercellular spaces and cells in the primary root–lateral root junction areas (Fig. 5B) and these were confirmed to be Zn-containing NPs by energy dispersive X-ray spectrometry (EDS) (Fig. S5†). These NPs and their aggregates were also observed in the surface and epidermis of roots (Fig. S6†).

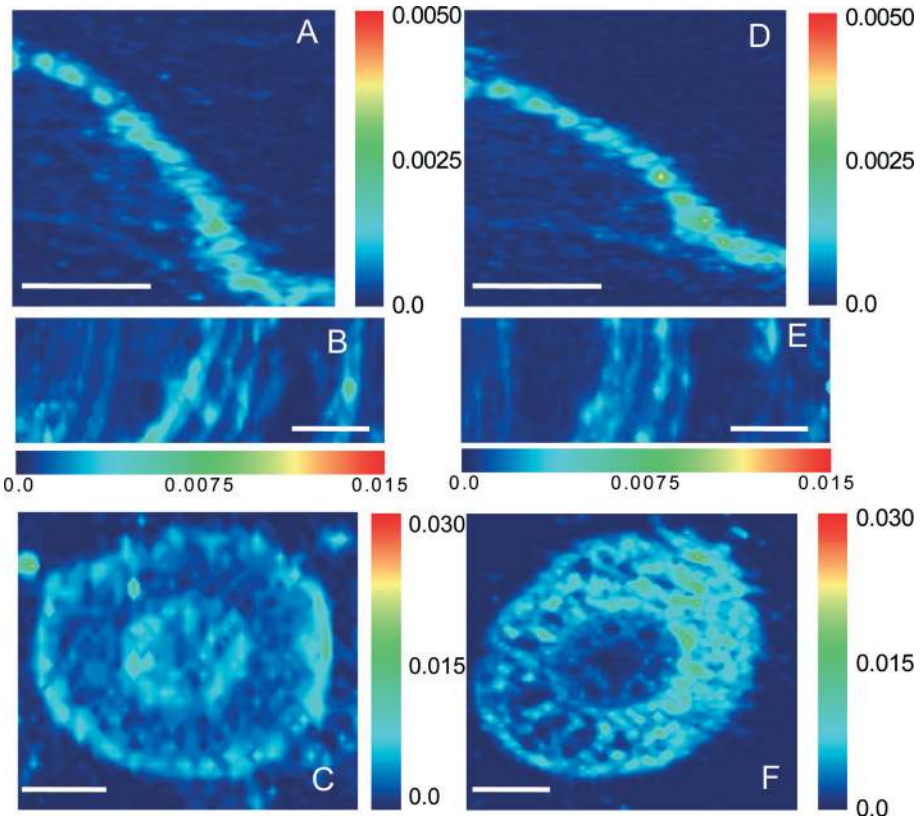

Fig. 3 Synchrotron μ-XRF microprobe imaging of Zn in leaf, stem, and root materials of maize seedlings exposed to 30 mg L^{-1} Zn^{2+} (A, B, C) and 100 mg L^{-1} ZnO NPs (D, E, F), respectively; scale bars represent 500 μm. The fluorescence yield counts collected were normalized by I_0 and dwell time. The red color was scaled to the maximum elemental concentration value for each map and the blue color was scaled to the minimum.

In addition, Zn-containing dense dots were also present in the apoplast, cytoplasm, membrane and vacuoles of some intact cells in the root tips (Fig. 5C and Fig. S7†), and even in the nuclei of cells with broken nuclear membranes (Fig. 5D) but were absent from the nuclei of cells with intact nuclear membranes (Fig. 5C and Fig. S7B†). Zn-containing dense dots were observed in the cells of maturation zones of roots, but their intensity was much weaker than that of root tips, with the exception of the primary root–lateral root junction areas (Fig. S8†).

4. Discussion

The overlap in Zn contents in plant tissues *vs.* dissolved Zn^{2+} concentration in ZnO NP and $ZnSO_4$ treatments (Fig. 1) reveals that Zn accumulation in maize was mainly determined by the actual Zn^{2+} concentration in the exposure suspensions. This conclusion was also supported by the evidence of the great similarity in both the *in situ* quantitative Zn distribution and Zn speciation in plant tissues (especially in shoots) obtained from μ-XRF maps (Fig. 3) and Zn K-edge XANES and EXAFS spectra (Fig. 2) of maize seedlings exposed to ZnO NPs and Zn^{2+}.

Synchrotron XAS analysis of the bulk plant samples indicates that Zn phosphate complexes were the major Zn species in all of the plant samples. Previous studies have found the conversion of Zn^{2+} ions to Zn phosphate in *Arabidopsis* grown hydroponically.[35,37–39] More recently, transformation of ZnO to Zn phosphate in wheat exposed to Zn NPs in a sand matrix has also been reported.[40] Nevertheless, differences in Zn coordinate structures between maize roots and shoots were found in the present study. Zn was present in a form more similar to amorphous Zn phosphate (Zn_{ads}-Phos) in roots, while Zn phosphate (hopeite or Zn phytate) was the major Zn species in shoots. Zhao *et al.* suggested that the formation of Zn phosphate in *Arabidopsis halleri* roots was mainly due to the co-precipitation of Zn and PO_4^{3-} on the rhizodermis, while Zn phosphate was not found in shoots.[38] Our results further confirm that the Zn phosphate species stored in maize roots was poorly crystallized, possibly due to the low PO_4^{3-} concentration in the exposure suspension (0.01 mmol L^{-1}). In contrast to Zn speciation in the roots, Zn accumulated in maize shoots mainly as hopeite/Zn phytate-like species. Hopeite is unlikely to be the main form in plant shoots because of the low PO_4^{3-} concentration in shoots. Therefore, it is reasonable to speculate that Zn phytate was likely the main species present in maize shoots because phytic acid (*myo*-inositol *kis*-hexaphosphate) is an effective chelator of cations such as calcium, zinc and iron,[41] and maize is among the cereal grains with high content of phytic acid.[42] However, the presence of hopeite cannot be excluded because of method limitations. Differences in Zn speciation between the

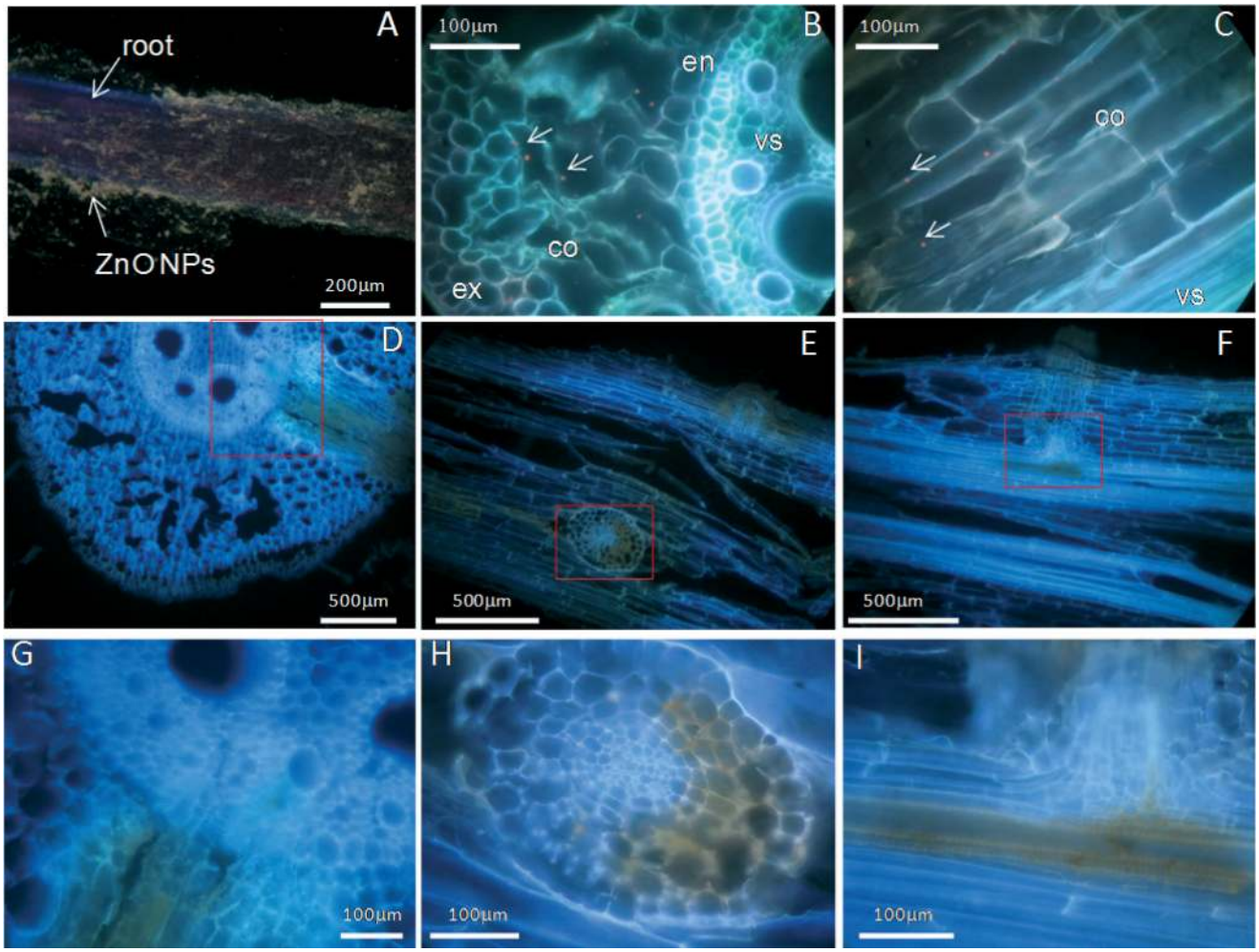

Fig. 4 Optical fluorescence microscopy images of ARS-ZnO NP adsorption on the root surface (A); the cross sections (B, D, G) and longitudinal sections (C, E, F, H, I) of maize roots exposed to ARS-ZnO NPs; (G), (H), and (I) are enlargements of the panes in (D), (E), (F), respectively; the exodermis (ex), cortex (co), endodermis (en) and vascular system (vs) are shown in (B) and (C).

Zn^{2+} and ZnO NP treatments were found only in root samples with a higher ZnO(H) percentage in roots treated with ZnO NPs, likely attributable to root surface adsorption of ZnO NPs and partial internalization of ZnO NPs in roots, as evidenced by fluorescence tracking and TEM. Whether or not those ZnO NPs internalized in roots can be transformed to Zn phosphate species inside maize during root-to-shoot transport needs further investigation.

Although it has been confirmed that Zn^{2+} from dissolution of ZnO NPs was the main (or perhaps the sole) source of Zn for maize uptake under treatment with ZnO NPs, we still cannot rule out the possibility of the entry and translocation of ZnO NPs in maize. ARS-labeled ZnO NPs (ARS-ZnO NPs) were used to track the distribution of ZnO NPs inside plants, which can provide macroscopic uptake and transport pathways of NPs in plants. In order to check whether the observed orange dots in plants were ARS-ZnO NPs or their aggregates, we examined the free ARS accumulated in roots. The free ARS appeared as a purple color, which was much different from the color of ARS-ZnO NPs (Fig. S4†). In addition, the content of the released dye from ARS-ZnO NPs in the exposure suspension was very limited (Fig. S9†); therefore, the potential influence of fluorescence emitted by plant uptake of free ARS and its complexation with calcium was negligible. ARS-ZnO NPs were observed inside the epidermis and cortex, but none was observed in the root vascular systems (Fig. 4B and C). This observation suggests that maize roots took up the ARS-ZnO NPs, but the endodermis prevented their entry into the root vascular systems. However, there was an interesting phenomenon that a much higher intensity of orange color was observed at the primary root–lateral root junction compared with other regions (Fig. 4D–I). At this specific location, ARS-ZnO NPs were even observed in the vascular cylinder of taproots (Fig. 4I), similar to the observation of FITC-stained ZnO NPs by Zhao *et al.*[27] Consistent observations were also obtained for bare ZnO NPs by μ-XRF mapping, which showed a much higher Zn accumulation in this area than that in the others (Fig. 6). TEM images further showed the presence of numerous Zn-containing dense dots in the intercellular space and cells of the primary

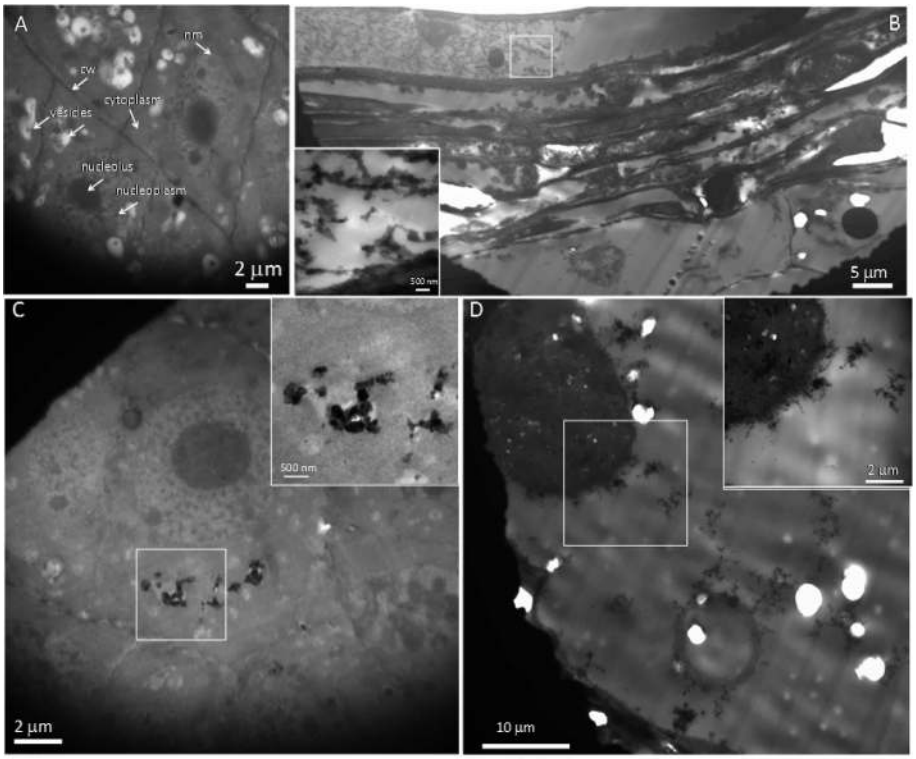

Fig. 5 TEM images of root tip sections of maize seedlings treated in blank (A) and primary root–lateral root junction of maize treated with 100 mg L^{-1} ZnO NPs (B); intact (C) and injured (D) cells in root tip sections under 100 mg L^{-1} ZnO NPs treatment; the inset is an enlargement of the pane in each figure.

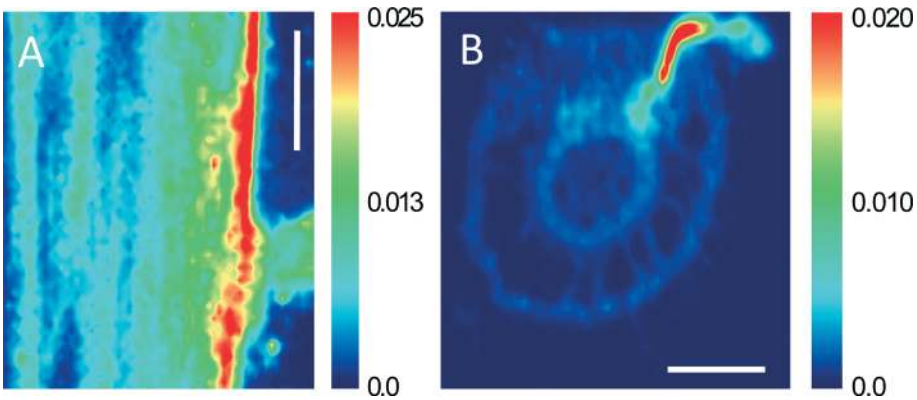

Fig. 6 Synchrotron μ-XRF mapping of longitudinal (A) and cross (B) sections of the maize root exposed to ZnO NPs, which reveals that a high level of Zn has accumulated in the area of the primary root–lateral root junction; bars represent 500 μm.

root–lateral root junction (Fig. 5B). Speciation analysis by XAFS and fluorescence labeling suggests that these dots shared the same features of ZnO NPs. In the mature zone of the roots, lignified cells left large vacant spaces for localization of NPs, and the abundant vessels of different sizes in the xylem provided available channels for the uptake of NPs with water flow. However, the Casparian strip, located in the transverse and radial walls of endodermal cells, forms a barrier to prevent the entry of macromolecules and particles into the vascular cylinder.[43] Therefore, the formation of the xylem Casparian strip is the key barrier for the entry of ZnO NPs. As shown in Fig. 4D and F, one terminal of the lateral root developed from the secondary xylem was in contact with the vascular cylinder of the primary root where the Casparian strip was disconnected (Fig. 4G and I),[44] thus providing an opportunity for NPs to traverse the membrane. Lateral root transmission is therefore speculated to be a plausible pathway for NPs to enter the vascular cylinder of the primary roots. TEM images demonstrate the internalized ZnO NPs in root cells at the area of root tips in maize after exposure to ZnO NPs. The main reason is that there is no exact morphological differentiation, and a Casparian strip has not formed

at the root tips. Further, both growth and division of cells in this zone are rapid.[45] NPs adsorbed on the surface of root tip cells were liable to be embedded in the intercellular space or enveloped inside the cells along with their fast division and growth. At the root tips, new cells are generated with root elongation. NPs internalized into surface cells were subsequently embedded by the new cells and present in the cells of other root zones, and thus have the opportunity to further enter the vascular cylinder of the primary roots through the junction regions of the primary root–lateral root. All results suggest that disconnection of the Casparian strip at the primary root–lateral root junction and an undeveloped Casparian strip combined with rapid cell growth and division at the root tips open a possible entry door for NPs at these specific locations.

No NPs were observed in maize shoots in this study by fluorescent tracking (Fig. S4D, E†) or TEM imaging (Fig. S8C, D†). Although there is a lack of substantial evidence to support or reject the upward translocation of ZnO nanoparticles in shoots due to methodological limitations, it is certain that the quantity of ZnO NPs entering the aerial parts of maize was very low if not zero. On the other hand, it would be expected that if some ZnO NPs enter plant roots they will be liable to undergo biotransformation to form Zn phosphate (mainly as Zn phytate) on their long-range upward transport pathway, an assertion that was supported by the observation that Zn existed mainly as Zn phosphate in the plant tissues. Such biotransformation will, as a result, prevent the upward translocation of ZnO NPs inside maize.

5. Conclusions

A comprehensive uptake pathway of ZnO NPs in maize is demonstrated based on observations from a combination of microscopic and spectroscopic techniques. Some of the ZnO NPs underwent dissolution in the exposure medium, which was enhanced as the result of root metabolic activities. The Zn^{2+} ions released from ZnO NPs were taken up by roots and accumulated in maize tissues mainly as Zn phosphate in both inorganic and organic forms. This is the main pathway for Zn uptake by maize. Simultaneously, a small fraction of ZnO NPs adsorbed on root surfaces enters the root cortex due to rapid cell division and elongation of the root tips, some of which enter the vascular systems through the gaps of the Casparian strip at the sites of the primary root–lateral root junction. Biotransformation of the ZnO NPs to Zn phosphate inside plants further limits their long-distance transport, resulting in negligible upward translocation of ZnO NPs into the shoots. Whether or not this nanoparticle uptake pathway that we propose is applicable to other nanoparticles and in the soil-plant system may merit further investigation. The results of this study highlight the importance of dissolution of ZnO NPs and the uptake of Zn^{2+} by plants, which indicates that our knowledge of plant uptake and phytotoxicity of Zn can to a large extent explain the interactions between ZnO NPs and plants.

Acknowledgements

This work was funded by the National Natural Science Foundation of China (projects 21277154 and 41023005) and the Strategic Priority Research Program of the Chinese Academy of Sciences (XDB14020202).

References

1 M. R. Wiesner, G. V. Lowry, P. Alvarez, D. Dionysiou and P. Biswas, *Environ. Sci. Technol.*, 2006, **40**, 4336–4345.
2 S. J. Klaine, P. J. J. Alvarez, G. E. Batley, T. F. Fernandes, R. D. Handy, D. Y. Lyon, S. Mahendra, M. J. McLaughlin and J. R. Lead, *Environ. Toxicol. Chem.*, 2008, **27**, 1825–1851.
3 A. Nel, T. Xia, L. Madler and N. Li, *Science*, 2006, **311**, 622–627.
4 E. Navarro, A. Baun, R. Behra, N. B. Hartmann, J. Filser, A. J. Miao, A. Quigg, P. H. Santschi and L. Sigg, *Ecotoxicology*, 2008, **17**, 372–386.
5 X. M. Ma, J. Geiser-Lee, Y. Deng and A. Kolmakov, *Sci. Total Environ.*, 2010, **408**, 3053–3061.
6 R. Nair, S. H. Varghese, B. G. Nair, T. Maekawa, Y. Yoshida and D. S. Kumar, *Plant Sci.*, 2010, **179**, 154–163.
7 T. Sabo-Attwood, J. M. Unrine, J. W. Stone, C. J. Murphy, S. Ghoshroy, D. Blom, P. M. Bertsch and L. A. Newman, *Nanotoxicology*, 2012, **6**, 353–360.
8 Z. Y. Wang, X. Y. Xie, J. Zhao, X. Y. Liu, W. Q. Feng, J. C. White and B. S. Xing, *Environ. Sci. Technol.*, 2012, **46**, 4434–4441.
9 J. E. Canas, M. Q. Long, S. Nations, R. Vadan, L. Dai, M. X. Luo, R. Ambikapathi, E. H. Lee and D. Olszyk, *Environ. Toxicol. Chem.*, 2008, **27**, 1922–1931.
10 S. Asli and P. M. Neumann, *Plant, Cell Environ.*, 2009, **32**, 577–584.
11 X. M. Tan, C. Lin and B. Fugetsu, *Carbon*, 2009, **47**, 3479–3487.
12 K. Birbaum, R. Brogioli, M. Schellenberg, E. Martinoia, W. J. Stark, D. Gunther and L. K. Limbach, *Environ. Sci. Technol.*, 2010, **44**, 8718–8723.
13 J. A. Hernandez-Viezcas, H. Castillo-Michel, A. D. Servin, J. R. Peralta-Videa and J. L. Gardea-Torresdey, *Chem. Eng. J.*, 2011, **170**, 346–352.
14 N. C. Carpita and D. M. Gibeaut, *Plant J.*, 1993, **3**, 1–30.
15 J. Kurepa, T. Paunesku, S. Vogt, H. Arora, B. M. Rabatic, J. J. Lu, M. B. Wanzer, G. E. Woloschak and J. A. Smalle, *Nano Lett.*, 2010, **10**, 2296–2302.
16 S. J. Lin, J. Reppert, Q. Hu, J. S. Hudson, M. L. Reid, T. A. Ratnikova, A. M. Rao, H. Luo and P. C. Ke, *Small*, 2009, **5**, 1128–1132.
17 R. Chen, T. A. Ratnikova, M. B. Stone, S. Lin, M. Lard, G. Huang, J. S. Hudson and P. C. Ke, *Small*, 2010, **6**, 612–617.
18 H. Zhu, J. Han, J. Q. Xiao and Y. Jin, *J. Environ. Monit.*, 2008, **10**, 713–717.
19 E. Corredor, P. S. Testillano, M. J. Coronado, P. Gonzalez-Melendi, R. Fernandez-Pacheco, C. Marquina,

M. R. Ibarra, J. M. de la Fuente, D. Rubiales, A. Perez-De-Luque and M. C. Risueno, *BMC Plant Biol.*, 2009, **9**, 45–53.
20 A. Hischemoller, J. Nordmann, P. Ptacek, K. Mummenhoff and M. Haase, *J. Biomed. Nanotechnol.*, 2009, **5**, 278–284.
21 N. Geldner, D. Roppolo, B. De Rybel, V. D. Tendon, A. Pfister, J. Alassimone, J. E. M. Vermeer, M. Yamazaki, Y. D. Stierhof and T. Beeckman, *Nature*, 2011, **473**, 380–384.
22 C. M. Rico, S. Majumdar, M. Duarte-Gardea, J. R. Peralta-Videa and J. L. Gardea-Torresdey, *J. Agric. Food Chem.*, 2011, **59**, 3485–3498.
23 D. X. Zhou and A. A. Keller, *Water Res.*, 2010, **44**, 2948–2956.
24 F. Gottschalk, T. Sonderer, R. W. Scholz and B. Nowack, *Environ. Sci. Technol.*, 2009, **43**, 9216–9222.
25 D. H. Lin and B. S. Xing, *Environ. Sci. Technol.*, 2008, **42**, 5580–5585.
26 M. L. Lopez-Moreno, G. de la Rosa, J. A. Hernandez-Viezcas, H. Castillo-Michel, C. E. Botez, J. R. Peralta-Videa and J. L. Gardea-Torresdey, *Environ. Sci. Technol.*, 2010, **44**, 7315–7320.
27 L. J. Zhao, J. R. Peralta-Videa, M. H. Ren, A. Varela-Ramirez, C. Q. Li, J. A. Hernandez-Viezcas, R. J. Aguilera and J. L. Gardea-Torresdey, *Chem. Eng. J.*, 2012, **184**, 1–8.
28 J. A. Hernandez-Viezcas, H. Castillo-Michel, J. C. Andrews, M. Cotte, C. Rico, J. R. Peralta-Videa, Y. Ge, J. H. Priester, P. A. Holden and J. L. Gardea-Torresdey, *ACS Nano*, 2013, **7**, 1415–1423.
29 Y. Yu, H. L. Huang, L. Luo, B. Wen and S. Z. Zhang, *J. Agric. Food Chem.*, 2009, **57**, 3695–3701.
30 E. Lombi, K. G. Scheckel, J. Pallon, A. M. Carey, Y. G. Zhu and A. A. Meharg, *New Phytol.*, 2009, **184**, 193–201.
31 G. Sarret, G. Willems, M. P. Isaure, M. A. Marcus, S. C. Fakra, H. Frerot, S. Pairis, N. Geoffroy, A. Manceau and P. Saumitou-Laprade, *New Phytol.*, 2009, **184**, 581–595.
32 M. Newville, *J. Synchrotron Radiat.*, 2001, **8**, 322–324.
33 T. Ressler, *J. Synchrotron Radiat.*, 1998, **5**, 118–122.
34 T. Rajh, L. X. Chen, K. Lukas, T. Liu, M. C. Thurnauer and D. M. Tiede, *J. Phys. Chem. B*, 2002, **106**, 10543–10552.
35 G. Sarret, P. Saumitou-Laprade, V. Bert, O. Proux, J. L. Hazemann, A. S. Traverse, M. A. Marcus and A. Manceau, *Plant Physiol.*, 2002, **130**, 1815–1826.
36 K. T. Thurn, T. Paunesku, A. G. Wu, E. M. B. Brown, B. Lai, S. Vogt, J. Maser, M. Aslam, V. Dravid, R. Bergan and G. E. Woloschak, *Small*, 2009, **5**, 1318–1325.
37 H. Kupper, E. Lombi, F. J. Zhao and S. P. McGrath, *Planta*, 2000, **212**, 75–84.
38 F. J. Zhao, E. Lombi, T. Breedon and S. P. McGrath, *Plant, Cell Environ.*, 2000, **23**, 507–514.
39 G. Sarret, J. Vangronsveld, A. Manceau, M. Musso, J. D'Haen, J. J. Menthonnex and J. L. Hazemann, *Environ. Sci. Technol.*, 2001, **35**, 2854–2859.
40 C. O. Dimkpa, D. E. Latta, J. E. McLean, D. W. Britt, M. I. Boyanov and A. J. Anderson, *Environ. Sci. Technol.*, 2013, **47**, 4734–4742.
41 V. Raboy, K. A. Young, J. A. Dorsch and A. Cook, *J. Plant Physiol.*, 2001, **158**, 489–497.
42 C. L. Adams, M. Hambidge, V. Raboy, J. A. Dorsch, L. Sian, J. L. Westcott and N. F. Krebs, *Am. J. Clin. Nutr.*, 2002, **76**, 556–559.
43 I. Karahara, A. Ikeda, T. Kondo and Y. Uetake, *Planta*, 2004, **219**, 41–47.
44 M. Mccully, *Plant Physiol.*, 1995, **109**, 1–6.
45 S. Doncheva, *J. Plant Physiol.*, 1998, **153**, 482–487.